Submitted to "STRAIN", November 2007

Revised version, February 2008

MULTIAXIAL SHAPE MEMORY EFFECT AND SUPERELASTICITY

K. LAVERNHE TAILLARD*, S. CALLOCH**, S. ARBAB CHIRANI***
and C. LEXCELLENT****

* LMT-Cachan, ENS de Cachan/CNRS-UMR 8535/Université Paris 6
61 avenue du Président Wilson, F-94235 Cachan Cedex, France
Tel : +33 (0)1 47 40 21 86, Fax : +33 (0)1 47 40 27 85
Corresponding author, e-mail : karine.lavernhe@lmt.ens-cachan.fr

** Laboratoire Brestois de Mécanique et des Systèmes, ENSIETA/UBO/ENIB
2 rue François Verny, F-29806 Brest Cedex 9, France
Tel : +33 (0)2 98 34 87 23, Fax : +33 (0)2 98 34 87 30

*** Laboratoire Brestois de Mécanique et des Systèmes, ENSIETA/UBO/ENIB
Technopôle Brest-Iroise, F-29280 Plouzané, France
Tel : +33 (0)2 98 05 66 81, Fax : +33 (0)2 98 05 66 53

**** FEMTO-ST, Département de Mécanique, UMR-CNRS 6174
24 chemin de l'Epitaphe, F-25000 Besançon, France
Tel : +33 (0)3 81 66 60 52, Fax : + 33 (0)3 81 66 67 00

MULTIAXIAL SHAPE MEMORY EFFECT AND SUPERELASTICITY

By K. Lavernhe Taillard, S. Calloch, S. Arbab Chirani and C. Lexcellent

ABSTRACT

The specific behavior of Shape Memory Alloys (SMA) is due to a martensitic transformation [1]. This transformation consists mainly in a shear without volume change and is activated either by stress or temperature. The superelastic behavior and the one way shape memory effect are both due to the partition between austenite and martensite.

The superelastic effect is obtained for fully austenitic SMA: loaded up to 5% strain, a sample recovers its initial shape after unloading with a hysteretic loop. The one way shape memory effect is obtained when a martensitic SMA, plastically deformed, recovers its initial shape by simple heating.

Superelasticity and one way shape memory effect are useful for several three-dimensional applications. Despite all these phenomena are well known and modeled in 1D, the 3D behavior, and especially the one way shape memory effect, remains quite unexplored [2]. Actually the development of complex 3D applications requires time consuming iterations and expensive prototypes. Predictive phenomenological models are consequently crucial objectives for the design and dimensioning of SMA structures.

Therefore, a series of 2D proportional and non-proportional, isothermal and non-isothermal tests has been performed. This database will be used to build a phenomenological model within the framework of irreversible processes.

Introduction

Among the various properties of SMA, several specificities are of great importance for their description. The first one is the coupling between mechanical and thermal behavior that is responsible for instance for the one way shape memory effect. Otherwise, the peculiar behavior during non proportional 3D mechanical loadings is due to the specific mechanism of martensite or R-phase reorientation. Moreover, the well-known tension-compression asymmetry has to be considered. Therefore the description of the specific behavior of SMA requires non isothermal models, able to take into account 3D proportional and non proportional loadings and the tension-compression asymmetry.

Many 3D constitutive macro-models describing the behavior of shape memory alloys were developed in the last ten years [3-9]. But very few of them are compared with non isothermal, non proportional 3D tests results. The main reason of it is the fact that very few complete test databases are available for SMA.

The present paper deals with experimental investigations on a textured nickel-titanium SMA. Both isothermal and anisothermal bi axial proportional and non proportional tests are performed. This database is then analyzed and an equivalent stress is defined.

Material

The polycrystalline nickel-titanium SMA (Ti-Ni 55.4 wt%) used for the tests was furnished by the *NDC* company. The samples have been obtained by drawing, then machined and heat treated (2 minutes in salt bath at 480°C) by the *Nitifrance* company. The transformation temperatures at free stress state have been determined using differential scanning calorimetry. Nevertheless, the experimental device was not able to reach sufficiently low temperature, to determine all characteristic transformation temperatures. Only R phase start temperature, R_s = 26°C, R phase finish temperature, R_f = 11°C, and austenite finish temperature, A_f = 30°C have been determined.

For this SMA the Young modulus at 50°C is in the order to E = 70 GPa, the Poisson ratio is $\nu = 0.3$ and the maximum transformation strain is estimated to $\varepsilon^M = 3\%$.

Experimental

The tests have been carried out on a MTS axial-torsion hydraulic testing machine. The axial and rotary actuators have a load capacity of 100 kN and 1.2 kN.m, respectively. Axial and shear strains were measured using a rosette-type strain gauge glued on the external diameter of the specimen. The samples are thin walled tubes; the geometry of the specimen is given on figure 1. A thermal chamber is also used for temperature regulation.

Isothermal case: superelasticity

SMA mechanicaly loaded for temperatures over Af presents a superelastic behavior : in a first step, the elasticity of austenite phase is observed, followed by a linearity lost denoting the beginning of the forward transformation (i.e., autenite to martentite). During unloading, the reverse transformation (i.e., martensite to austenite) occurs and is also followed by an elastic part. The specificity of superelasticity is the quasi absence of residual strain after unloading. The main objective of this part is to determine the shape of the initial transformation stress surface using an ad hoc experimental strategy. An automatic procedure, in a LabView environement, has been developed to detect the initial transformation onset surface. An interested reader can find all the details of this experimental procedure in [10]. The initial transformation onset surface is determined with a set of proportional loadings (i.e., radial loadings). During each proportionnal loading path, the equivalent stress-equivalent strain curve has been drawn. The elastic modulus is evaluated at the beginning of the curve and the transformation onset stress is defined when the equivalent transformation strain reaches a certain off-set. Then, values of corresponding axial stress, σ, and shear stress, τ, permit to define a point of the experimental transformation surface. In this work, the off-set of equivalent transformation strain is equal to 0.1%.

Nine proportional strain loading paths in tension-compression-torsion have been carried out at 50°C. Figure 2 shows the experimental shape of the initial transformation onset surface in the (σ,τ) plane. The material presents, on the one hand, a great tension-compression assymmetry (i.e., $\left|\sigma_y^c/\sigma_y^t\right| = 1.69$ where σ_y^c and σ_y^t are transformation onset stresses in compression and tension, respectively) and, on the other hand, a hight level of the

transformation onset stress in torsion (i.e., $\tau_y = 430\,\text{MPa}$). Indeed, for an isotropic SMA, the transformation onset stress in torsion, τ_y^{iso}, is related to σ_y^c and σ_y^t by the following relation [10]:

$$\tau_y^{iso} = \frac{\sigma_y^t}{\sqrt{3}} \frac{1}{cos\left(\frac{cos^{-1}(1-a)}{3}\right)} = 282\,\text{MPa} \tag{1}$$

Where a is a material parameter characterizing the tension-compression asymmetry and given by the following relation:

$$a = \frac{1 - cos\left(3\,cos^{-1}\left(\frac{\sigma_y^t}{\sigma_y^c}\right)\right)}{2} = 0.97 \tag{2}$$

The great difference between τ_y and τ_y^{iso} is due to the anisotropy of our SMA.

To modelize the experimental transformation surface, an equivalent stress has been defined. In this proposition, the isotropic equivalent stress proposed by Bouvet et al. [10-11] for isotropic SMA and given Eqs.(3-6) has been generalized to take into account the anisotropy of the material [12].

$$\sigma_{eq} = \sigma_{eq}(\bar{\sigma}, y_\sigma) = \bar{\sigma}.g(y_\sigma) \tag{3}$$

Where $\bar{\sigma}$ and y_σ are the second and the third stress invariants given by the following relations:

$$\bar{\sigma} = \sqrt{\frac{3}{2}\underline{\sigma}_D : \underline{\sigma}_D} \quad \text{with} \quad \underline{\sigma}_D = \underline{\sigma} - \frac{1}{3} trace(\underline{\sigma})\underline{I} \tag{4}$$

$$y_\sigma = \frac{27}{2}\frac{det(\underline{\sigma}_D)}{\bar{\sigma}^3} \tag{5}$$

and

$$g(y_\sigma) = \cos\left(\frac{\cos^{-1}(1 - a.(1 - y_\sigma))}{3}\right) \tag{6}$$

where the material parameter a is defined by Eq.(2).

A dilated stress tensor, denoted by $\underline{\widetilde{\sigma}}$, defined as a linear transformation of the stress tensor $\underline{\sigma}$, is introduced [13]:

$$\underline{\widetilde{\sigma}} = \underline{\underline{\underline{D}}}.\underline{\sigma} \tag{7}$$

where $\underline{\underline{\underline{D}}}$ contains constant material parameters.

This affine transformation $\underline{\underline{\underline{D}}}$ is chosen such as the Hill's hyper ellipsoid becomes a hyper sphere in the dilated stress space. The form of $\underline{\underline{\underline{D}}}$ is as following:

$$\underline{\underline{\underline{D}}} = \frac{1}{\nu}\begin{bmatrix} \frac{2A}{3}\cos^2(\varphi)+\frac{2B}{3}\sin^2(\varphi)+\frac{1}{3} & -\frac{A}{3}\cos^2(\varphi)-\frac{B}{3}\sin^2(\varphi)+\frac{1}{3} & -\frac{A}{3}\cos^2(\varphi)-\frac{B}{3}\sin^2(\varphi)+\frac{1}{3} & 0 & 0 & 0 \\ sym & \left(\frac{A}{6}+\frac{B}{2}\right)\cos^2(\varphi)+\left(\frac{A}{2}+\frac{B}{6}\right)\sin^2(\varphi)+\frac{1}{3} & \left(\frac{A}{6}-\frac{B}{2}\right)\cos^2(\varphi)+\left(\frac{B}{6}-\frac{A}{2}\right)\sin^2(\varphi)+\frac{1}{3} & 0 & 0 & 0 \\ sym & sym & \left(\frac{A}{6}+\frac{B}{2}\right).\cos^2(\varphi)+\left(\frac{A}{2}+\frac{B}{6}\right).\sin^2(\varphi)+\frac{1}{3} & 0 & 0 & 0 \\ 0 & 0 & 0 & \sqrt{L} & 0 & 0 \\ 0 & 0 & 0 & 0 & \sqrt{M} & 0 \\ 0 & 0 & 0 & 0 & 0 & \sqrt{N} \end{bmatrix} \tag{8}$$

with:

$$\begin{aligned} A^2 &= \alpha.\cos^2(\varphi) + \beta.\sin^2(\varphi) + \gamma.\cos(\varphi).\sin(\varphi) \\ B^2 &= \alpha.\sin^2(\varphi) + \beta.\cos^2(\varphi) - \gamma.\cos(\varphi).\sin(\varphi) \\ \varphi &= \frac{1}{2}.\arctan\left(\frac{\delta}{\beta - \alpha}\right) \\ \nu &= \sqrt{\frac{1}{2}\left[(D_{11} - D_{12})^2 + (D_{11} - D_{13})^2 + (D_{12} - D_{13})^2\right]} \end{aligned} \tag{9}$$

and:

$$\alpha = \frac{3}{2}.(F+H)$$
$$\beta = \frac{1}{2}F + \frac{1}{2}H + 2.G \qquad (10)$$
$$\delta = \sqrt{3}.(H-F)$$

where F, G, H, L, M, N are the Hill's criterion coefficients:

$$F(\sigma_{11}-\sigma_{22})^2 + G(\sigma_{22}-\sigma_{33})^2 + H(\sigma_{33}-\sigma_{11})^2 + 2L\sigma_{12}^2 + 2M\sigma_{23}^2 + 2N\sigma_{13}^2 = 1 \qquad (11)$$

The angle denoted φ, Eq. (9), corresponds to the inclination of the Hill's hyper ellipsoid in the stress space. Based on this linear transformation, an equivalent stress for anisotropic material, $\sigma_{eq\ ani}$, can be simply defined by substituting $\underline{\tilde{\sigma}}$ for $\underline{\sigma}$ in the equivalent stress defined by Eq.(3-6) for isotropic SMA:

$$\sigma_{eq\ ani} = \sigma_{eq\ ani}(\bar{\tilde{\sigma}}, y_{\tilde{\sigma}}) = \bar{\tilde{\sigma}}.g(y_{\tilde{\sigma}}) \qquad (13)$$

$$g(y_{\tilde{\sigma}}) = \cos\left(\frac{\cos^{-1}(1-a.(1-y_{\tilde{\sigma}}))}{3}\right) \qquad (14)$$

Where $\bar{\tilde{\sigma}}$ and y_σ are stress invariants of the dilated stress tensor $\underline{\tilde{\sigma}}$:

$$\bar{\tilde{\sigma}} = \sqrt{\frac{3}{2}\underline{\tilde{\sigma}}_D : \underline{\tilde{\sigma}}_D} \qquad (15)$$

$$y_\sigma = \frac{27}{2}\frac{\det(\underline{\tilde{\sigma}}_D)}{\bar{\tilde{\sigma}}^3} \qquad (16)$$

where $\underline{\tilde{\sigma}}_D$ is the deviatoric stress tensor of $\underline{\tilde{\sigma}}$.

This choice of a dilated stress tensor $\underline{\tilde{\sigma}}$ ensures the convexity of the equivalent stress whatever the parameters are: indeed the equivalent stress proposed by Bouvet et al. [10] is convex (demonstrated in [14]) and an affine transformation as $\underline{\underline{D}}$ is conservative for convexity [13].

An identification procedure [12] allows to determine the seven required parameters: $F=G=H=0.269\cdot10^{-5}$ (MPa^{-1}), $L=M=N=0.297\cdot10^{-5}$ (MPa^{-1}) and $a=0.97$. Then, the so identified equivalent stress is compared to the experimental transformation surface (Figure 2). The agreement between these two sets of data is good. The same method of identification performed for other anisotropic SMA for various loadings plans [12] shows that this anisotropic transformation surface is flexible enough to describe the whole set of possible experimental data.

Anisothermal case: one way shape memory effect

All the test presented in this section have been performed at –10°C. At this temperature, the alloy is in a R-phase state and has a pseudoplastic behavior under mechanical loading. This particular mechanical behavior is due to three successive deformation mechanisms (i.e., R-phase reorientation, R-phase distorsion and R-phase-martensite transformation, [15]).

In order to identify the surface of R-phase reorientation, a series of tests have been performed. Thirteen proportional loading paths have been performed in tension-compression-torsion. The procedure for the surface detection is the same as for superelasticity (i.e., presented in the previous section). The experimental results are given by the dots on Figure 3. The tension-compression asymmetry [16, 17] is very high (i.e., yield stress in compression is two times higher than the yield stress in tension) and this experimental results shows that this property is of crucial importance in SMA models.

This experimental surface for onset of reorientation is compared with the equivalent stress already identified in the case of superelasticity. The same values for the parameters are taken (no new identification is required), and the equivalent stress is reported on Figure 3 (continuous line). The agreement between the experimental results and the proposed model is very good. Consequently, the same equivalent stress can be used for 3D simulations for all temperatures.

To complete the database of non isothermal test, several one way shape memory effect tests were performed.

For each test, the sample is heated to 50°C to be fully austenitic, then cooled without stress to -10°C. The mechanical loading is then performed, at constant temperature. Loading is strain controlled at a strain rate of 5.10^{-5} s^{-1} and unloading is stress controlled (stress rate 1 $MPa.s^{-1}$) up to zero stress. Finally, always to zero stress, the sample is heated to 50°C.

Results obtained in tension during the ABCDE cycle are presented on Figure 4. Letters corresponds to the referenced points on each figure. Between A and B the sample is cooled without stress: the austenite is transformed into R-phase. This transformation is accompanied with a small deformation (0,1%) that corresponds to the thermal contraction. Between B and C, the sample is loaded in tension. In the first step, the R-phase reorientation takes place, followed by R-phase distortion. At the end, a plateau (partial here) is observed, corresponding to the transformation R-phase to oriented martensite [15]. The corresponding strain is irreversible at this temperature, as it can be seen after CD unloading. This CD unloading is linear and can be called elastic. Finally, between D and E, the sample is heated whereas the stress remains to zero. This heating is accompanied

between As and Af by the reverse transformation (oriented martensite to austenite) with progressive decline of the residual strain. The cycle is completely closed; indeed final state E is the same as the initial state A.

Results obtained in compression are not qualitatively different of those obtained in tension (Figure 5). Nevertheless quantitative differences during mechanical loading can be observed on Figure 6. This figure shows that the yield stress for the R-phase reorientation is very different (40 MPa versus 25 MPa in tension) and also that the necessary stress to obtained a certain strain is quite doubled; for instance 200 MPa versus 100 MPa in tension for a corresponding strain of 1.2%. To the contrary, during heating, the path is very similar.

In the same way, a torsion test is performed, reported on Figure 7. Between A and B, the material is cooled from 50°C to -10°C whereas stress is imposed to be zero ($\sigma = 0$ MPa and $\tau = 0$ MPa). Then mechanical loading at low temperature is strain controlled (e.g., axial strain $\varepsilon = 0\%$ whereas shear strain γ grows from 0% to 1,2%). The unloading CD is stress controlled (σ,τ) up to zero stress ($\sigma = 0$ MPa and $\tau = 0$ MPa). Finally the heating (-10°C to 50°C) is performed always at zero stress. Globally the behavior remains similar to the tension or compression. Yield stress for R-phase reorientation is estimated to 25 MPa in pure torsion; this value is higher than the von Mises equivalent stress corresponding to the yield stress for R-phase reorientation in tension (15 MPa).

Two other proportional tests are performed combining on one-hand tension and torsion loadings and on the other hand compression and torsion loadings (Figures 8 and 9). The way to control these tests remains similar. Between A and B, cooling from 50°C to -10°C without stress, then a proportional mechanical loading at low temperature (strain

controlled) is imposed. For the first loading path (tension-torsion), maxima for the strains are fixed to $\varepsilon = 1\%$ and $\gamma = 1{,}73\%$. For the second loading path (compression-torsion), they are fixed to $\varepsilon = -1\%$ and $\gamma = 1{,}73\%$. The mechanical unloading (CD segment) is stress piloted up to zero stress ($\sigma = 0$ MPa and $\tau = 0$ MPa). During heating (DE), stresses are maintained to zero. The same phenomena are always observed; notice particularly the quasi absence of residual strain after one complete cycle. This property was very useful to perform all the above-presented tests (tension, compression, torsion, tension-torsion and compression-torsion) on the same sample. The small residual strains observed for the last tests may be due to an education of the specimen after these five loading paths. It seems moreover that during heating (DE segment), the strain recovering occurs in "straight line" in the strain plane (ε,γ).

Conclusion

This paper is dedicated to an experimental database on an anisotropic Ni-Ti SMA. Anisothermal and bi-axial tension-compression-torsion proportional tests were performed. This kind of test database is the only one established for various temperatures and 2D loadings for the same SMA. This database has now to be used for the construction, identification and validation of a macroscopic model for SMA behavior.

Concerning the experimental observations, it can be noticed that:

- Taking into account the tension-compression asymmetry in the behavior for Ni-Ti SMA is of crucial importance; indeed the differences observed in tension and in compression are of the order of 50%.
- This tension-compression asymmetry is observed for yield stress surfaces during superelasticity (at temperature higher than A_f) denoting the beginning of the stress induced direct transformation (austenite to martensite) and also for yield stress surfaces during one way shape memory effect (at temperature lower than R_f and higher than M_s), when R-phase reorientation occurs.
- Furthermore, the shapes of the yield stress surfaces at different temperatures (i.e., 50°C and -10°C) are very similar. Indeed the associated equivalent stress proposed here is able to represent these both surfaces. We can so consider that the equivalent stress is consistent whatever the temperature is.
- Finally, bi-axial tension-compression-torsion proportional one way shape memory effect tests are presented and commented. These tests describe phenomena that should be taken into account in future models, as for instance the strain recovering during heating occurring in “straight line” in the strain plane (ε,γ).

References

1. Otsuka K., Wayman C.M. (1998) *Shape Memory Materials*. Cambridge University Press.
2. Tokuda, M., Sittner, P., Takakura, M. and Ye, M. (1995) Experimental study on performances in Cu-based shape memory alloy under multiaxial loading conditions. *Mat. Sc. Res. Int.* **1**, 260-265.
3. Helm, D. and Haupt, P. (2003) Shape memory behavior: modeling within continuum thermomechanics. *Int. J. of Sol. and Struct*. **40**, 827-849.
4. Juhasz, L., Schnack, E., Hesebeck, O. and Andrä, H. (2002) Macroscopic modeling of shape memory alloys under non-proportional thermo-mechanical loadings. *J. of Int. Mat. Syst. and Struct*. **13**, 825-836.
5. Lexcellent, C., Boubakar, M. L., Bouvet, C. et Calloch, S. (2006) About modeling the shape memory alloy behavior based on the phase transformation surface identification under proportional loading and anisothermal conditions. *Int. J. of Sol. and Struct*. **43**, 613-626.
6. Leclercq, S. and Lexcellent, C., (1996) A general macroscopic description of the thermomechanical behavior of shape memory alloys. *J. of Mech. and Phys. of Sol*. **44**, 953–980.
7. Auricchio, F. and Petrini, L., (2004) A three-dimensional model describing stress-temperature induced solid phase transformations. Part I: Solution algorithm and boundary value problems. *Int. J. for Num. Meth. in Eng*. **61**, 807–836.

8. Auricchio, F. and Petrini, L. (2004) A three dimensional model describing stress-temperature induced solid phase transformations. Part II: Thermomechanical coupling and hybrid composite applications. *Int. J. for Num. Meth. in Eng*. **61**, 716–737.
9. Lagoudas, D., Entchev, P., Popov, P., Patoor, E., Brinson, L. and Gao, X. (2006) Shape memory alloys, part II: Modelling of polycrystals. *Mech. of Mat*. **38**, 430–462.
10. Bouvet, C., Calloch, S. and Lexcellent, C. (2002) Mechanical behavior of a Cu-Al-Be shape memory alloy under multiaxial proportional and non proportional loadings. *J. Eng. Mat. and Techn.* **124**, 112-124.
11. Bouvet, C., Calloch, S. and Lexcellent, C. (2004) A phenomenological model for pseudoelasticity of shape memory alloys under multi-axial proportional and non-proportional loadings. *Eur. J. Mech. A Solids* **23**, 37-61.
12. Taillard, K., Arbab-Chirani, S., Calloch, S. and Lexcellent, C. (2008) Equivalent transformation strain and its relation with martensite volume fraction for isotropic and anisotropic shape memory alloys", *Mech. of Mat*. **40**, 151-170.
13. Barlat, F., Aretz, H., Yoon, J., Karabin, M. and Dick, R. (2005) Linear transformation-based anisotropic yield functions. *Int. J. of Plast*. **21**, 1009–1039.
14. Bigoni, D. and Piccolroaz, A. (2004) Yield criteria for quasibrittle and frictional materials. *Int. J. of Sol. and Struct.* **41**, 2855-2878
15. Sittner, P., Sedlak, P., Landa, M., Novak, V. and Lukas, P. (2006) In situ experimental evidence on R-phase related deformation processes in activated Ni-Ti wires. *Mat. Sc. and Eng. A* **438**, 579–584.

16. Gall, K., Sehitoglu, H., Chumlyakov, Y. and Kireeva, I. (1999) Tension-compression asymmetry on the stress-strain response in aged single crystal and polycrystalline NiTi. *Acta metal*. **47**, 1203–1217.
17. Gall, K., Sehitoglu, H. and Maier, H. (1997) Asymmetric stress-strain response in shape memory alloys. *Plast 97*, 153–154.

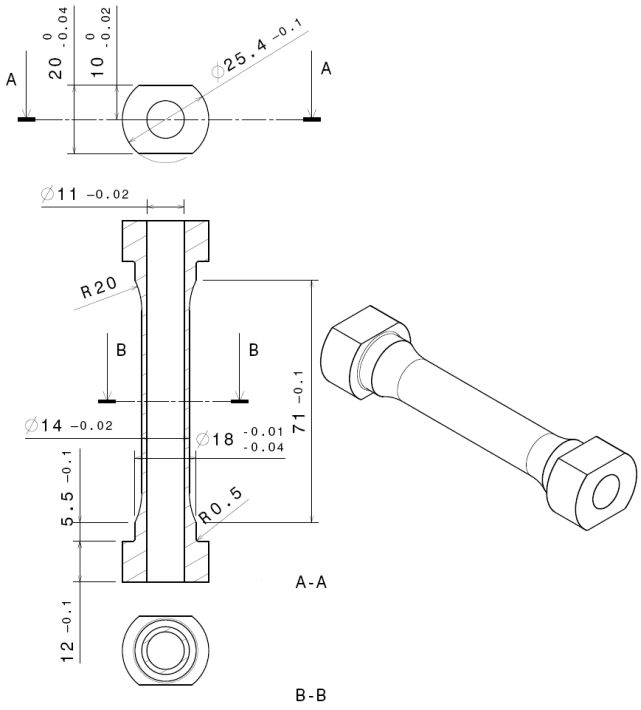

Figure 1. Tension-torsion thin walled tube specimen (in millimeters)

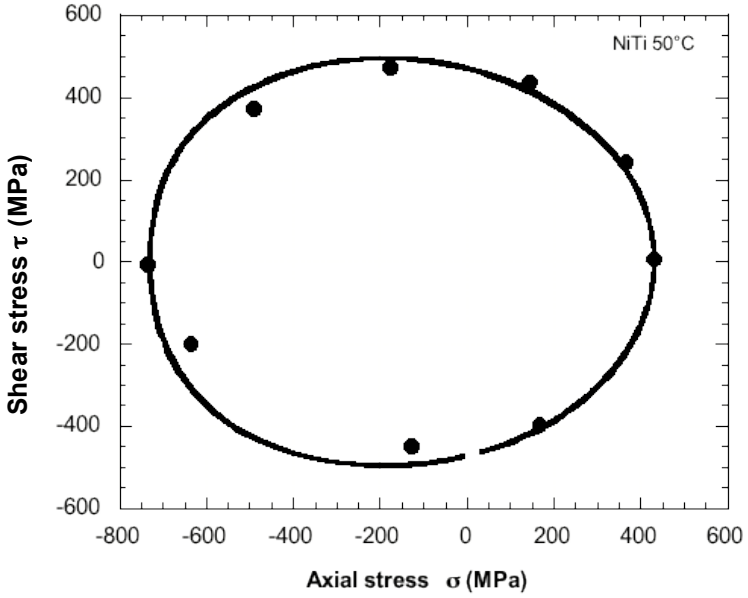

Figure 2. Tension-torsion “yield” stress surface for superelasticity: theoretical (continuous line) and experimental (dots)

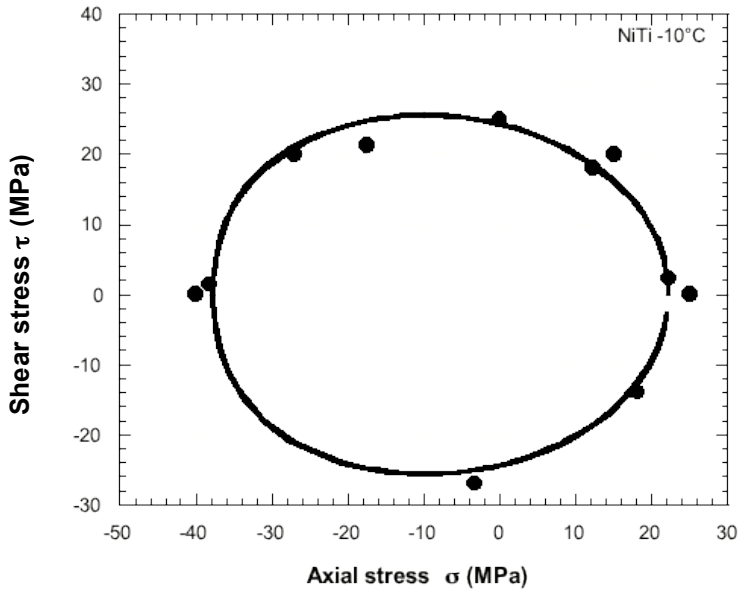

Figure 3. Tension-torsion “yield” stress surface for one way shape memory effect: theoretical (continuous line) and experimental (dots)

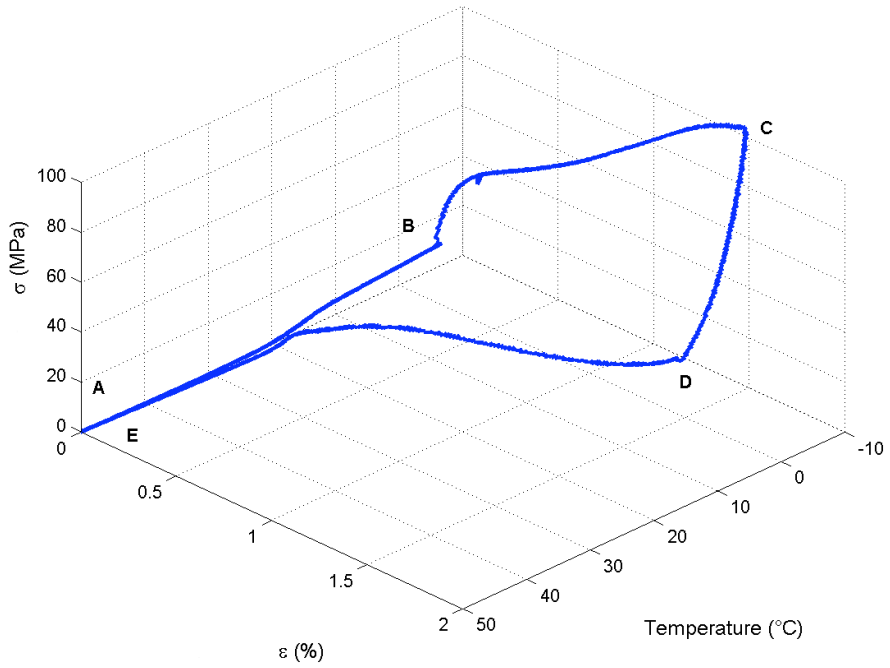

Figure 4. One way shape memory effect for pure tension

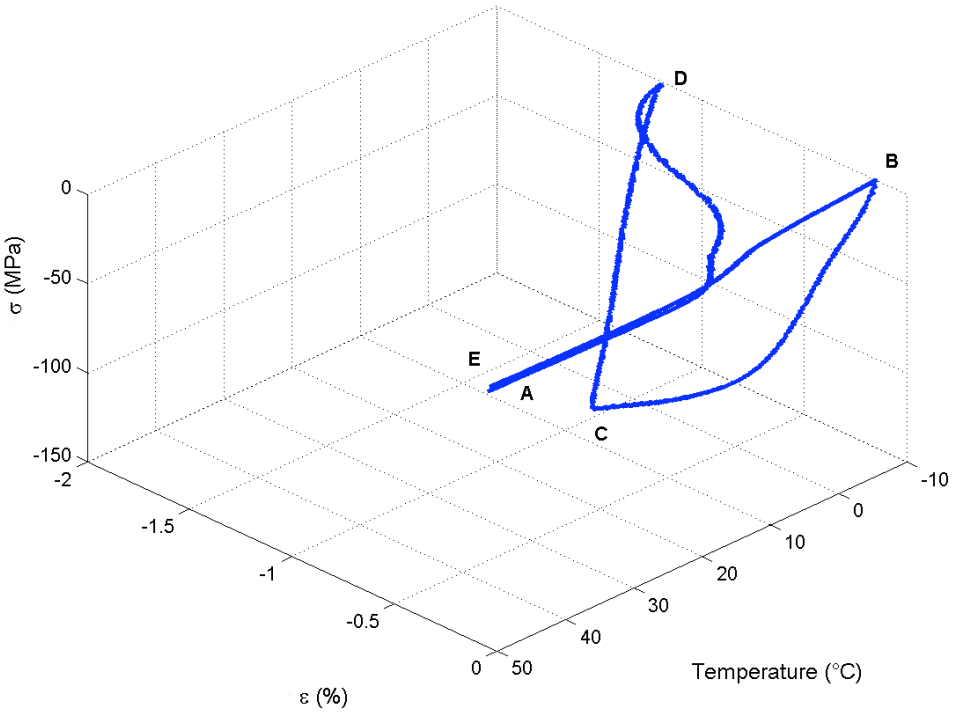

Figure 5. One way shape memory effect for pure compression

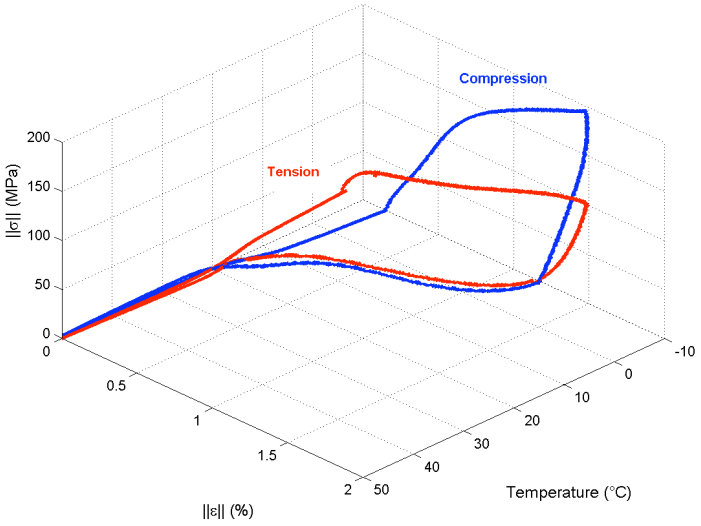

Figure 6. Comparison of one way shape memory effect for pure tension and compression

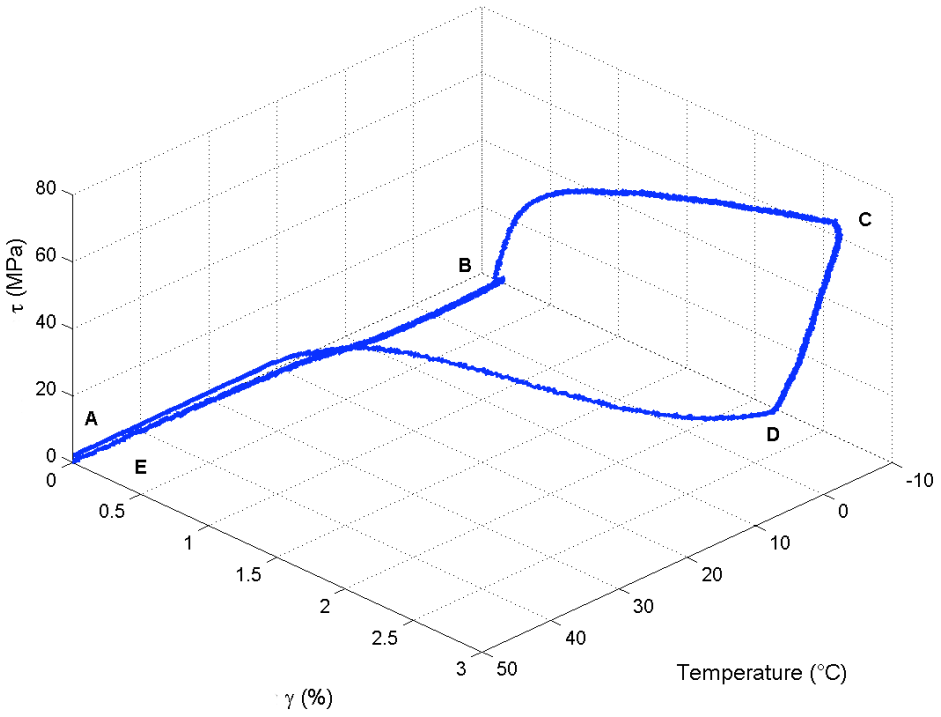

Figure 7. One way shape memory effect for pure torsion

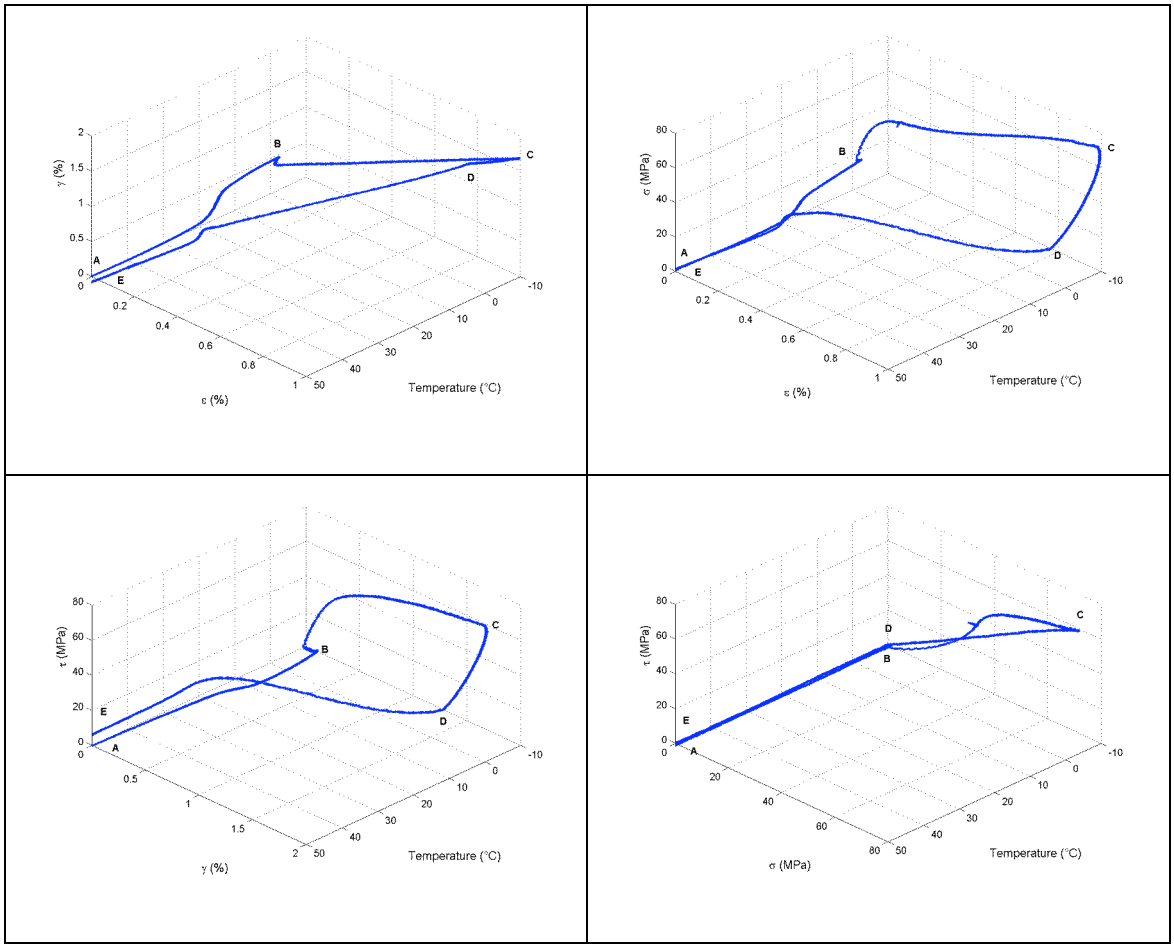

Figure 8. One way shape memory effect for combined tension-torsion loading

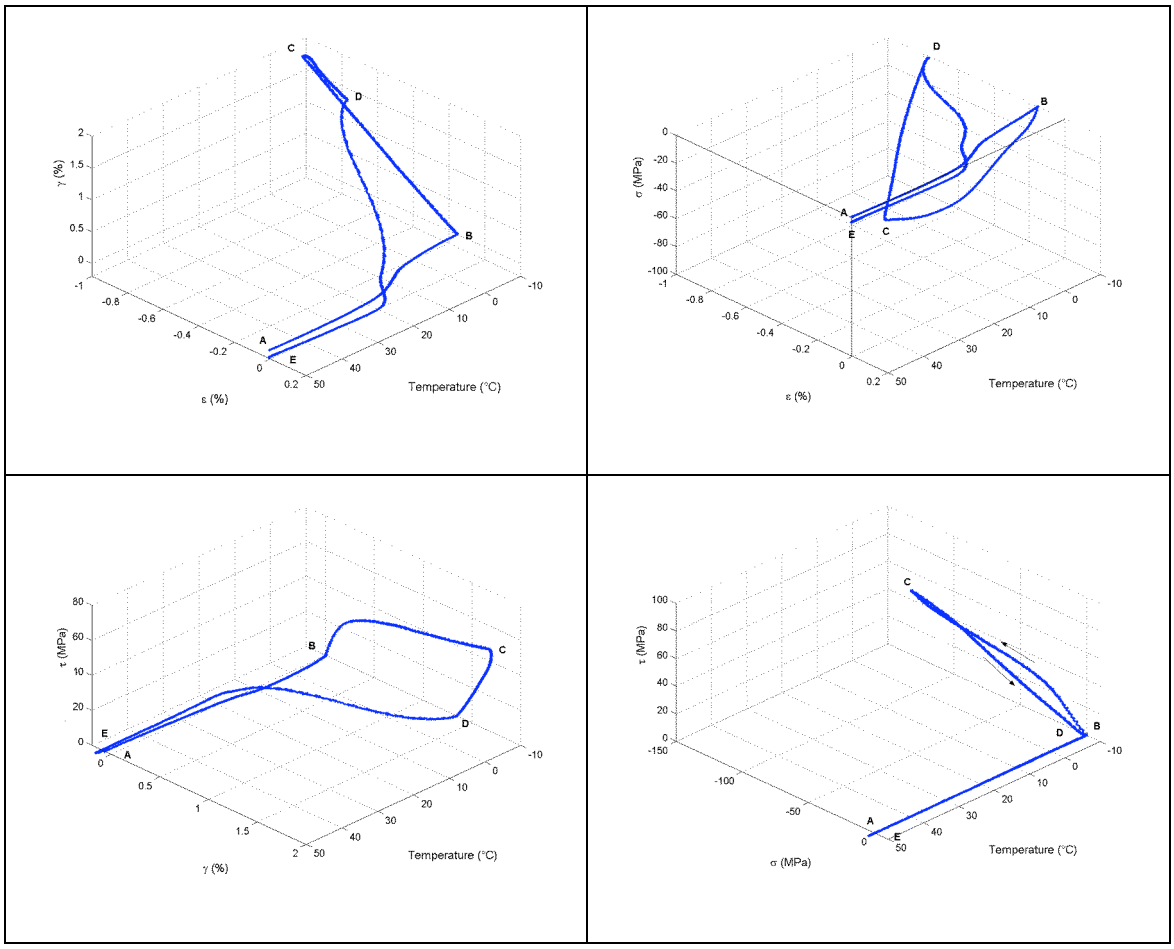

Figure 9. One way shape memory effect for combined compression-torsion loading